Photolysis of Gas-phase Atmospherically Relevant Monoterpene-derived Organic Nitrates

Yuchen Wang[†], Masayuki Takeuchi[‡], Siyuan Wang[#], Sergey A. Nizkorodov[&], Stefan France[§], Gamze Eris[†], Nga Lee Ng*[,†,¶,‡]

[†] School of Chemical and Bimolecular Engineering, Georgia Institute of Technology, Atlanta, Georgia 30332, USA
[‡] School of Civil and Environmental Engineering, Georgia Institute of Technology, Atlanta, Georgia 30332, USA
[&] Department of Chemistry, University of California, Irvine, California 92697, USA
[§] School of Chemistry and Biochemistry, Georgia Institute of Technology, Atlanta, Georgia 30332, USA
[#] Cooperative Institute for Research in Environmental Sciences (CIRES), University of Colorado, Boulder, CO and National Oceanic and Atmospheric Administration (NOAA), Chemical Sciences Laboratory (CSL), Boulder, CO
[¶] School of Earth and Atmospheric Sciences, Georgia Institute of Technology, Atlanta, Georgia 30332, USA
*Corresponding Author: Nga Lee Ng (ng@chbe.gatech.edu)

Abstract

Organic nitrates (ONs) can impact spatial distribution of reactive nitrogen species and ozone formation in the atmosphere. While photolysis of ONs is known to result in the release of NO_2 back to the atmosphere, the photolysis rate constants and mechanisms of monoterpene-derived ONs (MT-ONs) have not been well constrained. We investigated the gas-phase photolysis of three synthetic ONs derived from α-pinene, β-pinene, and d-limonene through chamber experiments. The measured photolysis rate constants ranged from $(0.55 \pm 0.10) \times 10^{-5}$ s^{-1} to $(2.3 \pm 0.80) \times 10^{-5}$ s^{-1} under chamber black lights. When extrapolated to solar spectral photon flux at a solar zenith angle of 28.14° in summer, the photolysis rate constants were in the range of $(4.1 \pm 1.4) \times 10^{-5}$ to $(14 \pm 6.7) \times 10^{-5}$ s^{-1} (corresponding to lifetimes of 2.0 ± 0.96 to 6.8 ± 2.4 h) and $(1.7 \pm 0.60) \times 10^{-5}$ to $(8.3 \pm 4.0) \times 10^{-5}$ s^{-1} (3.3 ± 1.6 to 17 ± 6.0 h lifetimes) by using wavelength-dependent and average quantum yields, respectively. Photolysis mechanisms were proposed based on major products detected during photolysis. A zero-dimensional box model was further employed to simulate the photolysis of α-pinene-derived ON under ambient conditions. We found that more than 99% of α-pinene-derived ON can be converted to inorganic nitrogen within 12 h of irradiation and ozone was formed correspondingly. Together, these findings show that photolysis is an important atmospheric sink for MT-ONs and highlight their role in NO_x recycling and ozone chemistry.

Keywords: Monoterpene, organonitrate, monoterpene nitrate, nitrogen budget, secondary organic aerosol, ozone, vapor wall loss.

1. Introduction

Air pollution is one of the biggest public health concerns across the globe.[1] Among different pollutants, nitrogen oxides (NO_x = NO + NO_2) are of particular interest owing to their capability to produce other secondary pollutants, such as ozone (O_3) and particulate nitrate. NO_x is emitted from a wide variety of anthropogenic sources such as fossil fuel combustion and industry.[2,3] In the atmosphere, NO_x can influence oxidation cycles of volatile organic compounds (VOCs) via photochemical reactions[3,4] initiated by hydroxyl radical (OH) and dark reactions[3,5] involving nitrate radical (NO_3) to produce organic nitrates (ONs). ONs are recognized to be major components of reactive oxidized nitrogen.[3,6,7] ONs can influence the NO_x cycle by serving as permanent sinks or temporary reservoirs of NO_x, and subsequently impact O_3 formation. Therefore, it is important to evaluate the kinetics and chemical mechanisms of loss processes of ONs in the atmosphere to understand their roles in NO_x recycling and O_3 formation.

Photolysis has been identified as a potential loss mechanism for ONs.[8–12] Photolysis can result in the direct release of NO_2 back to atmosphere by cleavage of nitrooxy group in ONs ($RONO_2 + h\nu \rightarrow RO + NO_2$). However, this process has not been well constrained owing to interferences from other processes such as reaction with atmospheric oxidants in field measurements and scarce photolysis information from laboratory experiments, especially for multifunctional ONs (*i.e.*, containing another functional group in addition to the nitrooxy group). Previous laboratory studies[8–11] on photolysis of multifunctional ONs have been limited to small alkyl carbonyl nitrates and alkyl hydroxy nitrates with 3-6 carbon atoms. The ambient photolysis lifetimes of small alkyl carbonyl nitrates have been shown to range from 0.5-9 h, which are comparable to other loss processes such as oxidation by OH[8–11,13–15] or hydrolysis.[16–23] There is no similar photolysis work for monoterpene-derived ONs (MT-ONs) in literature, although MT-ONs are prevalent in areas dominated by substantial biogenic–anthropogenic interactions such as in the southeastern U.S.[24–28] As a result, the treatment of photolysis of MT-ONs in current atmospheric models simply relies on analogies with structurally similar compounds (*e.g.*, tert-butyl nitrate) because of the paucity of direct laboratory measurements.[20,21,29,30] This is not a suitable model system as MT-ONs are almost always multifunctional by virtue of their formation mechanisms. Therefore, a thorough investigation of photolysis of MT-ONs is warranted to advance our understanding of monoterpene chemistry and improve their parameterizations in models for accurate predictions of their impacts.

In this work, we investigate the photolysis of three synthetic ONs derived from α-pinene, β-pinene, and d-limonene in laboratory chamber experiments. The chamber photolysis rate constants and the major photolysis products of these three MT-ONs are measured by high-resolution time-of-flight chemical ionization mass spectrometer (HR-ToF-CIMS). By comparing the solar and chamber spectral photon flux and the absorption cross sections of these synthetic MT-ONs measured by ultraviolet–visible (UV-Vis) spectrophotometry, the ambient photolysis rate constants are estimated. Photolysis mechanisms are

proposed to extend the previously reported photo-aging mechanisms for MT-ONs. Combining the proposed photolysis mechanisms and photolysis rate constants in a zero-dimensional (0-D) box model, we demonstrate the importance of photolysis of MT-ONs in NO_x recycling and O_3 formation under ambient conditions.

2. Experimental Section

2.1. Synthesis of monoterpene-derived ONs. Molecular structures of ONs synthesized in this work and their abbreviations are shown in Figure 1. The numbers (1°, 2°, and 3°) in the abbreviations denote a primary, secondary, and tertiary nitrooxy group, respectively. The synthetic strategies were the same as those reported in our previous study.[31] Briefly, commercially available monoterpene oxides (*i.e.*, α-pinene (Ap) oxide, d-limonene (Lm) oxide, and propylene oxide) directly react with fuming nitric acid (HNO_3) and undergo epoxide-opening reaction[32–34] to generate hydroxy nitrates (HN, *i.e.*, 2°_ApHN, 3°_ApHN, a mixture of 2°_LmHN and 3°_LmHN, and propylene-derived HN). Further oxidation of the hydroxyl group of hydroxy nitrates (*i.e.*, 2°_ApHN, 3°_LmHN, and propylene-derived HN) via the Dess-Martin oxidation[35] leads to the formation of keto-nitrates (KN, *i.e.*, 2°_ApKN, 3°_LmKN, and nitrooxyacetone (mixed with propylene-derived HN)). The halohydrination of the β-pinene (Bp) and d-limonene with N-bromosuccinimide[36,37] followed by nucleophilic substitution of the bromide with silver nitrate ($AgNO_3$)[15,38–40] can generate 1°_BpHN and 2°_LmHN, respectively.

Although nine ONs were synthesized in this study, only four of them (*i.e.*, 3°_ApHN, 2°_LmHN, 1°_BpHN, and nitrooxyacetone) were introduced into chamber to study the photolysis process. It is noted that the photolysis of 2°_ApHN, 2°_ApKN, and 3°_LmKN were not studied as they are solid compounds and we encountered difficulty in injecting them into the chamber owing to their low volatility. Also, we could not separate 3°_LmHN from its isomer 2°_LmHN. Although we could not separate nitrooxyacetone from propylene-derived HN as well (Figures S1 and S2), their different molecular masses as measured by HR-ToF-CIMS allowed us to study the photolysis process of nitrooxyacetone. To sum up, the photolysis process of 3°_ApHN, 2°_LmHN, 1°_BpHN, and nitrooxyacetone were studied by chamber experiments. Absorption spectra of 3°_ApHN, 3°_LmKN, 2°_ApKN, 2°_LmHN, and 1°_BpHN solutions were measured by a UV-Vis spectrophotometer (Cary 5000 UV-Vis/NIR, Agilent).

The purities of all synthetic ONs were higher than 99% based on nuclear magnetic resonance (NMR) spectra except 3°_ApHN (~98%) and 2°_ApHN (~95%). Pure standards were stored at -20 °C until use.

2.2. Chamber experiments. A series of experiments were performed at 295 ± 3 K in the Georgia Tech Environmental Chamber (GTEC) facility.[41] Prior to each experiment, the chamber was flushed with zero air (Aadco, 747-14) for at least 36 h. All experiments were carried out under dry conditions (<3% RH). No seed particle was added. The background concentrations of NO and NO_2 were less than 1 ppbv

for all experiments.

The photolysis of three synthetic MT-ONs (3°_ApHN, 2°_LmHN, and 1°_BpHN) and nitrooxyacetone were studied in chamber experiments. A 10 μL aliquot of ON in liquid form was transferred into a glass bulb, which was then evaporated and carried into the chamber by flowing zero air at 5 L min^{-1} through the bulb. The bulb was gently heated (around 313 K) to accelerate evaporation. The injection time was 1 h for 3°_ApHN and 1°_BpHN, and 20 min for 2°_LmHN and nitrooxyacetone. The MT-ON concentrations in the chamber were in the range of 2.7-7.8 ppbv, which were measured by a thermal dissociation cavity attenuated phase shift spectroscopy (TD-CAPS) (Table S2). Cyclohexane was added to the chamber (injection time: 30 min) as an OH scavenger with a mixing ratio of 10 ppmv, scavenging approximately 99% of OH radicals. Figure 2 shows the different time periods over the course of a typical experiment (2°_LmHN as an example). The dark period **D1** (started at about 20 min after the end of the cyclohexane injection) was to ensure that the chamber content was well-mixed and to evaluate the extent of vapor wall loss.[42–46] The experiment was initiated (time zero) by turning on the black lights surrounding the chamber (Sylvania, 24922). After 4-4.5 h of irradiation period, the MT-ON and its photolysis products were left in the dark for 1 h (**D2**) to evaluate vapor wall loss as well as reactions with photochemically generated O_3 (around 6-14 ppbv O_3 formed) and NO_3 radicals. Afterwards, 100 ppbv of NO from a standard cylinder (500 ppmv, Matheson) was injected into the chamber at 1 L min^{-1} to consume O_3 and NO_3 radicals. Since the MT-ONs studied in this work contain a double bond, this step prevents consumption of MT-ONs by O_3 and NO_3 radicals. The MT-ON and photolysis products were kept in the dark for another 40 min to 2 h (**D3**). Separate vapor wall loss experiments were also conducted for each MT-ON, in which the compound was injected into the chamber and kept in the dark (no lights) for 17 h to directly measure the vapor wall loss rate constant.

2.3. Instrumentation. The HR-ToF-CIMS (Aerodyne Research Inc.) used in this study has been described in previous literature.[13,47–49] Briefly, reagent ions are generated by flowing a mixture of CH_3I and dry N_2 (Airgas) through polonium-210 source (NRD; model P-2021). All the compounds presented in this study are I^- adducts. The instrument measures gaseous compounds by sampling air from the chamber at 1.7 L min^{-1}. In order to minimize changes in sensitivity due to varying water vapor pressure inside the ion molecule reactor (IMR), a small continuous flow of humidified N_2 (30–50 cm^3) through a bubbler at reduced pressure is continuously added to the IMR directly.[48] Each sampling cycle lasted for 30 min, consisting of 1 min of dry N_2 to capture baseline and 29 min of gas-phase sampling. The data were analyzed using Tofware v2.5.11.

The setting and the operation of TD-CAPS used in the experiments are similar to Sadanaga et al.[50] Briefly, the instrument has three channels connected to a CAPS monitor (Aerodyne Research Inc.) for NO_2 measurements. The reference channel measures the background NO_2 at room temperature in the

chamber. The other two channels have quartz tube reactors that are heated to 653 K and 473 K, which enable decomposition of alkyl nitrates and peroxy nitrates, respectively, to generate NO_2. The concentration of the injected ON in chamber was determined by the measured NO_2 difference under 653 K and room temperature. The quartz tube reactors were disconnected before chamber irradiation and only CAPS was used to measure the NO_2 in the chamber during photolysis. The 6 min sampling sequence used for CAPS included 1 min of zero gas to capture baseline and 5 min of chamber NO_2 sampling. A NO_x monitor (Thermo 42C) and an ultraviolet absorption O_3 monitor (Teledyne T400) were employed to measure NO and O_3, respectively.

2.4. Spectroscopic measurements. Absorption spectra of the MT-ON solutions (*i.e.*, 3°_ApHN, 3°_LmKN, 2°_ApKN, 2°_LmHN, and 1°_BpHN) were measured by a UV-Vis spectrophotometer with a 1 cm quartz cell. It is noted that the absorption spectra of 2°_ApHN, 3°_LmHN, propylene-derived HN, and nitrooxyacetone were not measured as we encountered difficulty in purifying 2°_ApHN to achieve high purity and in separating 3°_LmHN, propylene-derived HN, or nitrooxyacetone from the mixture. Ethyl ether was selected as the solvent as it has a relatively small polarity and reduces the solvent effect for absorption spectra.[51] Absorption spectra were recorded over a wavelength range of 200-800 nm. Only spectra of dissolved MT-ONs were determined, because a sufficiently sensitive gas-phase spectrophotometer was not available.

Molar extinction coefficient (ε_λ, L mol^{-1} cm^{-1}) was calculated from the Beer-Lambert law:

$$A_\lambda = \varepsilon_\lambda \times C \times l \quad (1)$$

where A_λ is the measured absorbance, C is the concentration of the absorber (mol L^{-1}), and l is the optical path length (1 cm).

The base-e absorption cross section (σ_λ, cm^2) was calculated from the equation:

$$\sigma_\lambda = \frac{\varepsilon_\lambda \times 10^3 \times ln(10)}{N_A} \quad (2)$$

where N_A is the Avogadro constant (6.022×10^{23} mol^{-1}). The measured absorption cross sections (average of 3-6 different solution concentrations) of MT-ONs are shown in Figures 3 and S5.

Photolysis rate constant (J) was calculated from the equation:

$$J = \int_{200\,nm}^{800\,nm} \sigma_\lambda(\lambda) \times F_\lambda(\lambda) \times Y_\lambda(\lambda) d\lambda, \quad (3)$$

where F_λ is the photon flux (photon s^{-1} cm^{-2} nm^{-1}) and Y_λ is the quantum yield, which is discussed in more detail below.

2.5. Zero-dimensional (0-D) box model. To better constrain the redistribution of N-containing species from MT-ON photolysis in both chamber and ambient conditions, a series of 0-D model simulations were performed using a box model previously described and used in Wang et al.[52,53] and references therein. This box model framework was written in IGOR Pro (WaveMetrics, Inc), which solves

the ordinary differential equations using the Backwards Differentiation Formula (BDF) method originally implemented in the CVODE package.[54] We simulated the photolysis of 3°_ApHN in the box model to estimate the levels of NO_x, inorganic nitrate (*i.e.*, HNO_3), and newly formed ONs as the total nitrogen produced from photolysis of 3°_ApHN. The chemical mechanism used in our work was the Master Chemical Mechanism (MCM, version 3.3.1), with our proposed photolysis mechanism of 3°_ApHN included. The rate constant for each reaction was predicted by either structure–activity relationships (SARs)[55,56] or MCM.[57–59] For chamber conditions, the photolysis rate constants for all related species (inorganic and organic species, *e.g.*, O_3, NO_2, acetic acid, etc.) were calculated through integrating their absorption cross sections and quantum yields reported in the MCM under GTEC chamber black lights. For ambient conditions, we extracted the solar spectral photon flux from tropospheric ultraviolet and visible TUV-radiation model (NCAR), August 1 at 33.7° latitude North (Atlanta, overhead O_3 column 300 Du, and albedo 0.1) from 7:00 am to 7:00 pm (Eastern Time). The average daytime solar zenith angle was 44.25°, which was employed in the MCM built-in function to normalize photolysis rate constants for all related species. The ambient photolysis rate constant of 3°_ApHN was estimated using the average daytime solar spectral photon flux of August 1 based on Equation 3. The details are discussed in section 3.3 and SI section S5.

3. Results and discussion

3.1. Photolysis of monoterpene-derived organic nitrates. Laboratory chamber experiments were performed to evaluate the photolysis rate constants for 3°_ApHN, 2°_LmHN, and 1°_BpHN. HR-ToF-CIMS was used to monitor the progress of reaction by monitoring the decay of normalized $C_{10}H_{17}NO_4I^-$ signal (ion cluster of I^- with MT-ONs). An example decay curve is shown in Figure 2 for 2°_LmHN. By plotting $\ln[C_{10}H_{17}NO_4I^-]_t/[C_{10}H_{17}NO_4I^-]_0$ as a function of time, a straight line can be fitted to the data in each period, with slope k_{UV} for the irradiation period and slopes k_{D1}, k_{D2}, and k_{D3} for the dark periods (Table S1). During irradiation, in addition to photolysis, OH oxidation, ozonolysis, NO_3 radical reaction, and vapor wall loss can contribute to the decay of the MT-ON. The OH oxidation pathway was eliminated with cyclohexane added to the chamber as an OH scavenger (Table S2). To determine the photolysis rate constant of MT-ON under chamber conditions ($J_{chamber}$), all other processes need to be accounted for. The methodology is detailed in Supporting Information section S2 and briefly noted here. The NO_3 radical reaction was negligible owing to the limited amount of NO_3 formed. The ozonolysis rate constant (k_{O3}) of each MT-ON was determined from separate ozonolysis experiment. The vapor wall loss rate constant (k_{vwl}) of each experiment was set to be the average of k_{D1} and k_{D3}, in which k_{D1} and k_{D3} are the vapor wall loss rate constants in **D1** and **D3** periods (before and after irradiation), respectively. The $J_{chamber}$ value was determined using a novel regression approach, in which the measured MT-ON time series data in the

irradiation period were fitted to the analytical solution of the differential equation describing the decay of MT-ON, considering photolysis, wall loss, and ozonolysis. Two experiments were conducted for each MT-ON. Results from the duplicate experiments were in good agreement (Figure S4). The photolysis rate constants (average of duplicate experiments) obtained for the three MT-ONs are given in Table 1.

Under GTEC chamber black lights, the photolysis rate constants were determined to be $J_{chamber}$ = (2.3 ± 0.80)×10^{-5} s^{-1} for 3°_ApHN, (1.3 ± 0.50)×10^{-5} s^{-1} for 2°_LmHN, and (0.55 ± 0.10)×10^{-5} s^{-1} for 1°_BpHN. The uncertainties of $J_{chamber}$ were calculated by propagating the statistical errors (2σ) associated with k_{vwl} and k_{O3}. Average quantum yields were determined by comparing the measured values of $J_{chamber}$ with predicted photolysis rate constants calculated by setting $Y_\lambda = 1$ in Equation 3 and using measured absorption cross sections and measured spectral photon flux (Figure 3). We obtained average quantum yields of 0.23, 0.071, and 0.038 for 3°_ApHN, 2°_LmHN, and 1°_BpHN, respectively (Table 1). These results suggest that MT-ONs have lower quantum yields than alkyl nitrates (3-5 carbon numbers), which have quantum yields of 0.9 or 1.0.[8–11] There are several explanations for the lower effective quantum yields of MT-ONs. It is possible that there is a solvatochromic shift between the absorption spectra we determined from solution-phase measurements and gas-phase absorption cross section – the extracted quantum yield would be quite sensitive to even a small shift. It is also likely that the larger MT-ONs are more efficiently quenched by O_2 and N_2 when photoexcited, which would decrease the photolysis quantum yield.[60] The impurity (<2%) in our synthetic MT-ONs can possibly lead to an overestimation of the absorption cross sections, and therefore reduction in the apparent quantum yields. The uncertainty in the measured chamber black lights spectra (5%, according to the instrument manuals, Figure 3a) can also affect the effective quantum yields. But the most important effect is that the quantum yield is not expected to be constant over the wavelength range of the chamber black lights. Since the wavelength dependence is not known, we assumed the simplest possible scenario with Y set to 1 below a certain cutoff wavelength and to 0 above this wavelength (similar to the well-known case of NO_2[61]). Using Equation 3 with unity quantum yield, we intergraded the absorption cross section of each MT-ON from 200 nm to a certain wavelength such that the calculated photolysis rate constant is equal to the measured photolysis rate constant. We regarded this specific wavelength as the cutoff wavelength for each MT-ON. We found that the cutoff wavelengths were 330 nm, 325 nm, and 312 nm for 3°_ApHN, 2°_LmHN, and 1°_BpHN, respectively (Table 1). We note that the assumed step-function dependence on wavelength is likely too simplistic, and future studies should measure the actual wavelength dependence of photolysis quantum yields for MT-ONs.

To extrapolate the chamber MT-ON photolysis rate constants to ambient conditions, one has to account for the difference between the spectral photon fluxes emitted by the chamber black lights and the sun (Figure 3). We estimated the ambient photolysis rate constants of these compounds using absorption

cross sections and cutoff wavelengths derived in this work and the solar spectral photon flux estimated by the TUV-radiation model at a solar zenith angle of 28.14° (12:00 solar time), August 1 at 33.7° latitude North (Atlanta, overhead O_3 column 300 Du, and albedo 0.1, Figure 3). Based on Equation 3, the ambient photolysis rate constants were estimated to be $(8.3 \pm 4.0)\times10^{-5}$ s^{-1} for 3°_ApHN, $(3.0 \pm 1.5)\times10^{-5}$ s^{-1} for 2°_LmHN, and $(1.7 \pm 0.60)\times10^{-5}$ s^{-1} for 1°_BpHN using the average quantum yields. The corresponding lifetimes were 3.3 ± 1.6 h, 9.2 ± 4.5 h, and 17 ± 6.0 h for 3°_ApHN, 2°_LmHN, 1°_BpHN, respectively. When employing the wavelength-dependent quantum yield for each MT-ON, the ambient photolysis rate constants were $(14 \pm 6.7)\times10^{-5}$ s^{-1} for 3°_ApHN, $(8.1 \pm 4.0)\times10^{-5}$ s^{-1} for 2°_LmHN, and $(4.1 \pm 1.4)\times10^{-5}$ s^{-1} for 1°_BpHN, with corresponding lifetimes of 2.0 ± 0.96 h, 3.4 ± 1.7 h, and 6.8 ± 2.4 h, respectively (Table 1). The uncertainties of ambient photolysis rate constants and corresponding lifetimes of MT-ONs were propagated from $J_{chamber}$, instrumental uncertainty (5%) of measured chamber spectral photon flux, and uncertainty of the average of measured absorption cross sections from different solution concentrations (Figure 3b).

Nitrooxyacetone was used as a reference compound to compare our results with previous work.[8,10,11] Under GTEC chamber black lights, the photolysis rate constant of nitrooxyacetone was determined to be $(0.29 \pm 0.11)\times10^{-5}$ s^{-1}, corresponding to a lifetime of 95 ± 36 h. Owing to the limitation in our synthetic method, we could not separate pure nitrooxyacetone to measure its absorption cross section. Thus, we used the reported absorption cross section for nitrooxyacetone[12,62] to estimate its photolysis rate constant under chamber conditions. The calculated average quantum yield for nitrooxyacetone was 0.50 ± 0.21, which is lower than previously reported (0.9 or 1.0).[10,11] This difference could arise from the use of relatively short chamber experiments (4 h) to estimate photolysis rate constant of nitrooxyacetone, which has a long lifetime (95 h).

According to previous work, interactions between the two adjacent functional groups can strongly affect the absorption cross sections. [8–12,63] The conjugation of carbonyl group and nitrooxy group can lead to a larger absorption cross section at atmospherically relevant wavelengths (*i.e.,* above 290 nm). [8–12,63] In this work, we also measured the absorption cross sections of 2°_ApKN and 3°_LmKN (Figure S5). The absorption cross section of 3°_LmKN is higher than other MT-ONs at wavelengths above 270 nm, which can be explained by the conjugation of carbonyl group and nitrooxy group. By comparing the absorption cross sections of 3°_ApHN, 2°_ApKN, and 2°_LmHN, we found that the conjugation of double bond and hydroxyl group (3°_ApHN) can also increase the absorption intensity from wavelengths 220-270 nm compared to single carbonyl group (2°_ApKN) or single nitrooxy group (2°_LmHN). We also found that the conjugation of double bond and nitrooxy group can enhance the absorption cross section of 1°_BpHN from wavelengths 220-270 nm. Taken together, these results show that 1) the enhancement in absorption cross section from the conjugation effect between carbonyl group with nitrooxy group (3°_LmKN) is the

highest at wavelengths above 270 nm and 2) the conjugation of double bond and nitrooxy group (1°_BpHN) or hydroxyl group (3°_ApHN) can increase the absorption cross section from wavelengths 220-270 nm.

While we could not measure the photolysis rate constants of 2°_ApKN and 3°_LmKN in chamber experiments owing difficulty in injecting them into the chamber, we evaluated their ambient photolysis rate constants by Equation 3 using the wavelength-dependent quantum yields (Table S4) obtained from chamber photolysis experiments of 1°_BpHN, 2°_LmHN, and 3°_ApHN. The ambient photolysis lifetimes were estimated to be 2.3-7.9 h for 2°_ApKN and 0.69-3.1 h for 3°_LmKN.

The reported photolysis rate constants for MT-ONs in this work are much faster than those reported for alkyl hydroxy nitrates with 3-6 carbons,[15] but of the same order of magnitude as alkyl keto-nitrates with 3-5 carbons [8–11] (Figure 4). In previous studies, photolysis was reported to be the dominant sink for alkyl keto-nitrates with lifetimes less than 9 h (Table S3). The short photolysis lifetimes of MT-ONs were attributed to the synergetic interaction between the nitrooxy group and double bond or carbonyl group to increase the $\pi \rightarrow \pi^*$ and $n \rightarrow \pi^*$ transition intensities. We found that the absorption cross sections of MT-ONs are higher than smaller alkyl keto-nitrates (*e.g.*, nitrooxy acetone, Figure S5), which can be explained by absorption cross sections increasing with longer carbon chain length.[64] Although future work is warranted to ascertain the photolysis rate constants for all kinds of MT-ONs with multifunctional groups, our results indicate that photolysis has the potential to be a substantial sink for MT-ONs.

3.2. Photolysis products and mechanisms. The major gas-phase products from photolysis of 3°_ApHN, 2°_LmHN, and 1°_BpHN were measured by HR-ToF-CIMS (Figures 5a, S9a, and S10a). The dominant gas-phase product was $C_{10}H_{17}NO_5$ for all three MT-ONs. For 3°_ApHN, other major gas-phase products were $C_7H_{10}O_3$ and $C_{10}H_{16}O_3$ (Figure 5a). For 1°_BpHN (Figure S10a), other major gas-phase products were $C_7H_{10}O_3$, $C_9H_{14}O_3$, $C_7H_{11}NO_5$, and $C_9H_{15}NO_5$. Interestingly, we noticed that $C_7H_{10}O_3$ from 3°_ApHN and $C_{10}H_{17}NO_5$ from 2°_LmHN increased during both irradiation and **D2** periods. Because of the presence of NO_3 radicals and large amount of O_3 in **D2** period, the increase in **D2** period can be attributed to ozonolysis and/or NO_3 radical reaction of the MT-ONs. However, we observed a much faster generation rate during irradiation period than **D2** period, indicating that photolysis was a more efficient formation pathway than ozonolysis and/or NO_3 radical reaction. Vapor wall loss led to the decrease of products during **D3** (without light, NO_3 radicals and O_3) period.

Figure 5b shows the proposed formation mechanism of major products from photolysis of 3°_ApHN as observed by HR-ToF-CIMS. 3°_ApHN is the first-generation oxidation product from α-pinene/OH reaction in the presence of NO.[65] The photolysis process started as reaction R1 with the O-N bond cleavage. The RO can simultaneously undergo (1) isomerization because of the double bond via reaction R2, (2) decomposition via reaction R3, and (3) 1,5 H-migration via reactions R4 and R5. While we could

not obtain the branching ratio directly through the ratio of products from R2, R3, R4, and R5, we used structure–activity relationships[55,56] to estimate the rate constant for R3, R4 and R5, which was determined to be 3.61×10^{8} s^{-1}, 1.02×10^{7} s^{-1}, and 6.65×10^{7} s^{-1}, respectively. There is no direct method to evaluate the isomerization rate constant of RO. However, according to Vereecken et al.,[66,67] the potential energy barrier for decomposition of RO (5.2 kcal/mol) to eliminate acetone (reaction R3) is similar to isomerization (5.0 kcal/mol) to form six membered cyclic ether (reaction R2). Thus, we assumed the branching ratio for isomerization, decomposition, and 1,5 H-migration was 0.45:0.45:0.1. O_2 combines with the alkyl radicals from R2, R3, R4, and R5 to generate peroxy radicals (RO_2) quickly. Therefore, we regarded alkyl radical formation and O_2 addition as one step. C10RO2 from reaction R2 (isomerization), M1C10RO2 from R4 (1,5 H-migration), and M2C10RO2 from R5 (1,5 H-migration) can further react with NO from the chamber background or from photolysis of NO_2 to produce $C_{10}H_{17}NO_5$. $C_{10}H_{17}NO_5$ has been commonly detected in field measurements and chamber experiments from reaction of monoterpene with NO_3 radicals.[27,41,48,68] It is noted that the $C_{10}H_{17}NO_5$ generated from R5 is unstable because of the special structure with hydroxyl and nitrooxy group linked in one carbon atom. This work provided an alternative pathway for $C_{10}H_{17}NO_5$ formation through photolysis of monoterpene-derived hydroxy nitrates. Alternatively, C10RO2 and M1C10RO2 can be oxidized to generate ketone compound $C_{10}H_{16}O_3$. Simultaneously, C7RO2 from reaction R3 (decomposition) produced $C_7H_{10}O_3$ through several steps with NO and any of the radicals present (RO_2 or HO_2).

The proposed photolysis mechanisms for 2^o_LmHN and 1^o_BpHN are shown in Figures S9b and S10b, respectively. In these mechanisms, RO produced by direct photolysis of 1^o_BpHN also underwent isomerization, decomposition, and 1,5 H-migration to produce the major photolysis products. However, RO produced by photolysis of 2^o_LmHN can only undergo decomposition and 1,5 H-migration because of the stereo-structure. Specifically, the oxy radical and allyl group are located on different spatial surfaces, which prevents the isomerization of RO formed from 2^o_LmHN photolysis. As the mass spectrometer provides formulas but no structural information, the product structures shown in the figures are tentative, and multiple isomeric products may be possible. In addition, we only reported photolysis reaction of MT-ONs with RO and NO_2 as the major products. Elimination reactions or photoisomerization reactions may potentially be minor pathways in photolysis mechanisms of MT-ONs and warrant future studies.

3.3. Modeling results. In order to evaluate the influence of MT-ONs photolysis on NO_x recycling and O_3 formation, we employed a 0-D box model to simulate photolysis of 3^o_ApHN under both chamber and ambient conditions. Since I-CIMS tends to have a higher selectivity towards compounds with higher oxygen numbers and its sensitivity can differ widely between compounds,[69–71] some products with fewer oxygen numbers or with higher detection limits may not have been detected during photolysis. Therefore,

we included all possible products in the MCM photolysis mechanism of 3°_ApHN and major products detected by I-CIMS (Figure S11) in the following model simulations. In model simulations of chamber conditions, the OH reaction, NO_3 radical reaction and ozonolysis rate constants for 3°_ApHN were 9.9×10^{-10} cm^3 $molecule^{-1}$ s^{-1}, 7.2×10^{-12} cm^3 $molecule^{-1}$ s^{-1} and 4.2×10^{-17} cm^3 $molecule^{-1}$ s^{-1}, respectively, which were estimated by MCM and separate ozonolysis experiment. The photolysis rate constant was 2.4×10^{-5} s^{-1} and vapor wall loss rate constant was 2.9×10^{-5} s^{-1}, which was the average of k_{D1} and k_{D3} (Section S3). The model results were sensitive to the initial NO level, hence we conducted two sets of model simulations with an initial NO concentration of 0 versus 1 ppbv. The simulated 3°_ApHN, O_3, and NO_2 were in good agreement with our measurements in both cases (Figure S13). The measured O_3 level was 14 ppbv at the end of photolysis. When including the O_3 source in chamber (0.02 ppbv/min from chamber background experiment, Figure S12), the level of O_3 during irradiation matched the simulated O_3 range considering instrument uncertainty. The measured NO_2 level was consistent with simulated NO_2 considering instrument uncertainty.[72] For NO, because it was difficult to capture 0.1 ppbv change of NO in the NO_x monitor during photolysis experiments (the detection limit of the NO_x monitor is 0.4 ppbv), we did not observe any dynamic trend of NO in the experiments (the model predicted that NO was below 0.4 ppbv most of the time). The average measured NO concentration was 0.94 ppbv.

The agreement between our experimental observations and model simulations under chamber conditions allowed us to extend the model simulations from chamber conditions to ambient conditions. The initial concentration of 3°_ApHN was set to be 28 pptv. This concentration was roughly determined based on the reported daily average α-pinene concentration (0.37 ppbv)[49] and the yield to produce 3°_ApHN from OH-initiated oxidation of α-pinene (upper bound as 7.5%, which is the yield of ring-opened RO_2 which can further react with NO to produce 3°_ApHN, MCM) (SI Section S5.4). In this work, we employed the box model to simulate the simplest case with photolysis as the only sink for 3°_ApHN. The model simulation started with 3°_ApHN as the only reactive nitrogen source, without any initial NO and NO_2.[49] We did not consider the OH reaction, NO_3 radical reaction, and ozonolysis of 3°_ApHN. In ambient conditions, the photolysis rate constant of 3°_ApHN was determined to 10.2×10^{-5} s^{-1}. It is noted that this value is different from the photolysis rate constant of 3°_ApHN discussed in section 3.1, which is for 12:00 solar time. Here, we used the twelve-hour average solar spectral photon flux (7:00 am to 7:00 pm, Eastern time) in Atlanta of August 1 to estimate the photolysis rate constant of 3°_ApHN (Figure S14) with wavelength-dependent quantum yield. The initial O_3 concentration was 46 ppbv (summer average in Atlanta, https://www.epa.gov/outdoor-air-quality-data/download-daily-data). The other relevant parameters (*e.g.*, relative humidity, temperate, etc.) employed in the model are detailed in the SI (section S5.4).

The simulation was run for 12 h and the results are shown in Figure 6. Released from photolysis of

3°_ApHN, NO_2 can undergo fast photolysis to produce NO and O_3. NO can produce new ONs by reaction with RO_2. Therefore, the NO_x/ONs cycle essentially served as a NO_x reservoir, extending the effective lifetime of NO_x which would otherwise be oxidized to HNO_3. After 12 h of irradiation, the reactive nitrogen from the initial 3°_ApHN was converted into NO_x (2.7% mass of reactive nitrogen), inorganic nitrate (*i.e.*, gaseous HNO_3, 97%), and a small fraction (0.36%) remained in the form of ONs. Along with the nitrogen conversion during photolysis of 3°_ApHN, O_3 increased (0.34 ppbv). This increase of O_3 is a result of the photolysis of NO_2 (released from 3°_ApHN photolysis).

4. Atmospheric implication

Monoterpenes, a major class of biogenic volatile organic compounds, are known to react with OH radical under high NO_x condition and NO_3 radical to produce MT-ONs.[3,24–27] Among them, MT-ONs with hydroxyl group are typical first-generation products.[47,65,73] In this study, we experimentally determined the photolysis rate constants of three MT-ONs with hydroxyl groups (*i.e.*, 3°_ApHN, 2°_LmHN, and 1°_BpHN) in chamber experiments. By comparing the photolysis rate constants predicted from the measured absorption cross sections with the measured photolysis rate constants of MT-ONs from chamber experiments, we extrapolated the chamber MT-ONs photolysis rate constants to ambient conditions using either average quantum yields or wavelength-dependent quantum yields. The results from this work alone do not allow for evaluation of which quantum yield is more accurate. However, wavelength-dependent quantum yields are more commonly observed for photolysis of atmospherically relevant species (*e.g.*, NO_2[61], acetaldehyde[74], etc.). The ambient photolysis lifetimes for 3°_ApHN, 2°_LmHN and 1°_BpHN were determined to be 2.0 ± 0.96 h, 3.4 ± 1.7 h, and 6.8 ± 2.4 h, respectively, using wavelength-dependent quantum yields. It is noted that we assumed the simplest possible scenario in which the quantum yield is 1 below a certain cutoff wavelength and 0 above this wavelength. This assumption can lead to overestimation of the ambient photolysis rate constants and underestimation of the photolysis lifetimes of MT-ONs.

The photolysis lifetimes of MT-ONs were shorter than those for smaller alky nitrates, which can be attributed to the larger absorption cross sections in these MT-ONs, which likely arise from the synergy between chromophoric functional groups (e.g., double bond, nitrooxy group).[57] We found that the enhancement in absorption cross section from the conjugation effect between carbonyl group with nitrooxy group (3°_LmKN) is the highest at wavelengths above 270 nm. The conjugation of double bond and nitrooxy group (1°_BpHN) or hydroxyl group (3°_ApHN) can increase the absorption cross section from wavelengths 220-270 nm.

In addition, we proposed formation mechanisms for the major photolysis products of 3°_ApHN and 1°_BpHN, which were produced by RO isomerization, decomposition and 1,5 H-mitigation. However, the major photolysis product of 2°_LmHN was only produced by RO decomposition and 1,5 H-mitigation. The

isomerization of RO (ring closure) was less studied compared to RO decomposition and H-mitigation.[55,56] Although efficient RO isomerization (ring closure) typically requires the RO to have an unsaturated bond,[66] previous work revealed that RO with an unsaturated bond is one of the major intermediates in the reactions of isoprene[75] or terpenes[3,76] with OH or NO_3 radicals. Therefore, it is worth studying the rate constant of isomerization of RO (ring closure) with an unsaturated bond and OH substituent in future, which can be the missing pathway in isoprene or terpenes oxidation by OH and NO_3 mechanisms.[65–67,77]

In addition to photolysis, MT-ONs can undergo other loss pathways such as OH reaction and ozonolysis. To evaluate the relative importance of photolysis of MT-ONs in ambient conditions with respect to other loss processes, we compared the photolysis lifetimes with those from gas-phase OH reaction and ozonolysis (estimated by MCM, Estimation Program Interface suite[78], and separate ozonolysis experiments) for 3°_ApHN, 2°_LmHN, and 1°_BpHN. The lifetimes for OH reaction ([OH] = 1.5×10^6 molecule cm^{-3}) and ozonolysis ([O_3] = 50 ppbv) for these MT-ONs ranged from 1.9-3.2 h and 5.3-20 h, respectively (Table 2). The photolysis, OH reaction, and ozonolysis lifetimes of MT-ONs in gas phase are comparable, demonstrating that photolysis is a competitive loss process for MT-ONs.

The treatment of photolysis of MT-ONs in current atmospheric models simply relies on analogies with structurally similar compounds.[20,21,29,30] For example, Browne et al. (2014)[30] reported that 3-6% of degradation of MT-ONs was caused by photolysis. In their global chemical transport model, Browne et al. set the photolysis rate constant of MT-ONs to be one third of the photolysis rate constant of tert-butyl nitrate, which was 5-42 times smaller than our reported photolysis rate constants of MT-ONs under the same solar spectral photon flux. This means the loss rate for MT-ONs was underpredicted in the model. Schwantes et al. (2020)[29] estimated that less than 10% loss of MT-ONs was due to photolysis, when employing the photolysis rate constant of methyl hydroperoxide to represent the photolysis rate constant of MT-ONs. The photolysis rate constant of methyl hydroperoxide was 3-20 times smaller than our reported photolysis rate constants of MT-ONs under the same solar spectral photon flux. Therefore, the degradation fraction of MT-ONs by photolysis and the subsequent O_3 formation can be different when using our reported photolysis rate constants of MT-ONs. In this work, we only employed a simple box model to simulate the simplest case in the atmosphere with photolysis as the only sink for 3°_ApHN. After 12 h of irradiation time, 99% of 3°_ApHN was converted to inorganic nitrogen with O_3 formation. This simplest model simulation indicates that the photolysis of MT-ONs can be one of the sources of NO_x for O_3 formation and photolysis is an important atmospheric sink for MT-ONs. This is the first study to report experimentally constrained photolysis rate constants of MT-ONs, which provides the fundamental information to update MT-ON chemistry in regional and global chemical transport models. The MT-ONs reported in this work are limited to unsaturated, less-oxygenated compounds ($C_{10}H_xNO_4$) while ambient MT-ONs have more diverse chemical structures and are more oxygenated ($C_{10}H_xNO_{>4}$; multifunctional,

saturated/unsaturated, etc.).[27,49,79] Future photolysis studies on such diverse MT-ONs are warranted to obtain a more comprehensive understanding on their impacts on nitrogen/NO_x recycling and O_3 budget as a whole system.

Supporting Information

The supporting information is available free of charge via the Internet at http://pubs.acs.org. Additional details on methods, calculation of MT-ON photolysis rate constants and vapor wall loss rate constants, literature review of previous ON photolysis studies, photolysis mechanisms, and parameters used in the 0D-model is in supporting information. The measured absorption cross sections of MT-ONs and chamber experiment data are available online at the Index of Chamber Atmospheric Research in the United States (ICARUS, https://icarus.ucdavis.edu/).

Acknowledgements

The authors would like to acknowledge financial support by the National Science Foundation (NSF) CAREER AGS-1555034 and the National Oceanic and Atmospheric Administration (NOAA) NA18OAR4310112. SAN acknowledges support from NSF grant AGS-1853639. The HR-ToF-CIMS was purchased through NSF Major Research Instrumentation (MRI) grant 1428738. The author would also like to acknowledge Dr. Yuanlong Huang for helpful discussions of vapor wall loss and Tianchang Xu for helpful comments on the manuscript.

References:

(1) Pope, C. A.; Dockery, D. W.; Schwartz, J. Review of Epidemiological Evidence of Health Effects of Particulate Air Pollution. *Inhal. Toxicol.* **1994**, 137–331. https://doi.org/10.3109/08958378.2011.593587.

(2) Crutzen, P. A Discussion of the Chemistry of Some Minor Constituents in the Stratosphere and Troposphere. *Pure Appl. Geophys.* **1973**, *106–108* (1), 1385–1399. https://doi.org/10.1007/BF00881092.

(3) Ng, L. N.; Brown, S. S.; Archibald, A. T.; Atlas, E.; Cohen, R. C.; Crowley, J. N.; Day, D. A.; Donahue, N. M.; Fry, J. L.; Fuchs, H. et al. Nitrate Radicals and Biogenic Volatile Organic Compounds: Oxidation, Mechanisms, and Organic Aerosol. *Atmos. Chem. Phys.* **2017**, *17* (3), 2103–2162. https://doi.org/10.5194/acp-17-2103-2017.

(4) Chameides, W. L. The Photochemical Role of Tropospheric Nitrogen Oxides. *Geophys. Res. Lett.* **1978**, *5* (1), 17–20.

(5) Winer, A. M.; Atkinson, R.; Pitts, J. N. Gaseous Nitrate Radical: Possible Nighttime Atmospheric Sink for Biogenic Organic Compounds. *Science (80-.).* **1984**, *224* (4645), 156–159. https://doi.org/10.1126/science.224.4645.156.

(6) Perring, A. E.; Bertram, T. H.; Farmer, D. K.; Wooldridge, P. J.; Dibb, J.; Blake, N. J.; Blake, D. R.; Singh, H. B.; Fuelberg, H.; Diskin, G. et al. The Production and Persistence of ΣRONO2 in the Mexico City Plume. *Atmos. Chem. Phys.* **2010**, *10* (15), 7215–7229. https://doi.org/10.5194/acp-10-7215-2010.

(7) Perring, A. E.; Pusede, S. E.; Cohen, R. C. An Observational Perspective on the Atmospheric Impacts of Alkyl and Multifunctional Nitrates on Ozone and Secondary Organic Aerosol. *Chem. Rev.* **2013**, *113* (8), 5848–5870. https://doi.org/10.1021/cr300520x.

(8) Picquet-Varrault, B.; Suarez-Bertoa, R.; Duncianu, M.; Cazaunau, M.; Pangui, E.; David, M.; Doussin, J. F. Photolysis and Oxidation by OH Radicals of Two Carbonyl Nitrates: 4-Nitrooxy-2-Butanone and 5-Nitrooxy-2-Pentanone. *Atmos. Chem. Phys.* **2020**, *20* (1), 487–498. https://doi.org/10.5194/acp-20-487-2020.

(9) Xiong, F.; Borca, C. H.; Slipchenko, L. V.; Shepson, P. B. Photochemical Degradation of Isoprene-Derived 4,1-Nitrooxy Enal. *Atmos. Chem. Phys.* **2016**, *16* (9), 5595–5610. https://doi.org/10.5194/acp-16-5595-2016.

(10) Müller, J. F.; Peeters, J.; Stavrakou, T. Fast Photolysis of Carbonyl Nitrates from Isoprene. *Atmos. Chem. Phys.* **2014**, *14* (5), 2497–2508. https://doi.org/10.5194/acp-14-2497-2014.

(11) Suarez-Bertoa, R.; Picquet-Varrault, B.; Tamas, W.; Pangui, E.; Doussin, J. F. Atmospheric Fate of a Series of Carbonyl Nitrates: Photolysis Frequencies and OH-Oxidation Rate Constants. *Environ. Sci. Technol.* **2012**, *46* (22), 12502–12509. https://doi.org/10.1021/es302613x.

(12) Barnes, I.; Becker, K. H.; Zhu, T. Near UV Absorption Spectra and Photolysis Products of Difunctional Organic Nitrates: Possible Importance as NOx Reservoirs. *J. Atmos. Chem.* **1993**, *17* (4), 353–373. https://doi.org/10.1007/BF00696854.

(13) Nah, T.; Sanchez, J.; Boyd, C. M.; Ng, N. L. Photochemical Aging of α-Pinene and β-Pinene Secondary Organic Aerosol Formed from Nitrate Radical Oxidation. *Environ. Sci. Technol.* **2016**, *50* (1), 222–231. https://doi.org/10.1021/acs.est.5b04594.

(14) Lee, L.; Teng, A. P.; Wennberg, P. O.; Crounse, J. D.; Cohen, R. C. On Rates and Mechanisms of OH and O3 Reactions with Isoprene-Derived Hydroxy Nitrates. *J. Phys. Chem. A* **2014**, *118* (9), 1622–1637. https://doi.org/10.1021/jp4107603.

(15) Treves, K.; Rudich, Y. The Atmospheric Fate of C3-C6 Hydroxyalkyl Nitrates. *J. Phys. Chem. A* **2003**, *107* (39), 7809–7817. https://doi.org/10.1021/jp035064l.

(16) Darer, A. I.; Cole-Filipiak, N. C.; O'Connor, A. E.; Elrod, M. J. Formation and Stability of Atmospherically Relevant Isoprene-Derived Organosulfates and Organonitrates. *Environ. Sci. Technol.* **2011**, *45* (5), 1895–1902. https://doi.org/10.1021/es103797z.

(17) Hu, K. S.; Darer, A. I.; Elrod, M. J. Thermodynamics and Kinetics of the Hydrolysis of Atmospherically Relevant Organonitrates and Organosulfates. *Atmos. Chem. Phys.* **2011**, *11* (16), 8307–8320. https://doi.org/10.5194/acp-11-8307-2011.

(18) Rindelaub, J. D.; Borca, C. H.; Hostetler, M. A.; Slade, J. H.; Lipton, M. A.; Slipchenko, L. V.; Shepson, P. B. The Acid-Catalyzed Hydrolysis of an α-Pinene-Derived Organic Nitrate: Kinetics, Products, Reaction Mechanisms, and Atmospheric Impact. *Atmos. Chem. Phys.* **2016**, *16* (23), 15425–15432. https://doi.org/10.5194/acp-16-15425-2016.

(19) Pye, H. O. T.; Luecken, D. J.; Xu, L.; Boyd, C. M.; Ng, N. L.; Baker, K. R.; Ayres, B. R.; Bash, J. O.; Baumann, K.; Carter, W. P. L. et al. Modeling the Current and Future Roles of Particulate Organic Nitrates in the Southeastern United States. *Environ. Sci. Technol.* **2015**, *49* (24), 14195–14203. https://doi.org/10.1021/acs.est.5b03738.

(20) Fisher, J. A.; Jacob, D. J.; Travis, K. R.; Kim, P. S.; Marais, E. A.; Miller, C. C.; Yu, K.; Zhu, L.; Yantosca, R. M.; Sulprizio, M. P. et al. Organic Nitrate Chemistry and Its Implications for Nitrogen Budgets in an Isoprene- and Monoterpene-Rich Atmosphere: Constraints from Aircraft (SEAC4RS) and Ground-Based (SOAS) Observations in the Southeast US; *Atmos. Chem. Phys.* **2016**, *16*, 5969–5991. https://doi.org/10.5194/acp-16-5969-2016.

(21) Zare, A.; Romer, P. S.; Nguyen, T.; Keutsch, F. N.; Skog, K.; Cohen, R. C. A Comprehensive Organic Nitrate Chemistry: Insights into the Lifetime of Atmospheric Organic Nitrates. *Atmos. Chem. Phys.* **2018**, *18* (20), 15419–15436. https://doi.org/10.5194/acp-18-15419-2018.

(22) Zare, A.; Fahey, K. M.; Sarwar, G.; Cohen, R. C.; Pye, H. O. T. Vapor-Pressure Pathways Initiate but Hydrolysis Products Dominate the Aerosol Estimated from Organic Nitrates. *ACS Earth Sp. Chem.* **2019**, *3* (8), 1426–1437. https://doi.org/10.1021/acsearthspacechem.9b00067.

(23) Vasquez, K. T.; Crounse, J. D.; Schulze, B. C.; Bates, K. H.; Teng, A. P.; Xu, L.; Allen, H. M.; Wennberg, P. O. Rapid Hydrolysis of Tertiary Isoprene Nitrate Efficiently Removes NOx from the Atmosphere. *Proc. Natl. Acad. Sci. U. S. A.* **2021**, *117* (52), 33011–33016. https://doi.org/10.1073/PNAS.2017442117.

(24) Xu, L.; Guo, H.; Boyd, C. M.; Klein, M.; Bougiatioti, A.; Cerully, K. M.; Hite, J. R.; Isaacman-VanWertz, G.; Kreisberg, N. M.; Knote, C. et al. Effects of Anthropogenic Emissions on Aerosol Formation from Isoprene and Monoterpenes in the Southeastern United States. *Proc. Natl. Acad. Sci.* **2015**, *112* (1), 37–42. https://doi.org/10.1073/PNAS.1417609112.

(25) Xu, L.; Suresh, S.; Guo, H.; Weber, R. J.; Ng, N. L. Aerosol Characterization over the Southeastern United States Using High-Resolution Aerosol Mass Spectrometry: Spatial and Seasonal Variation of Aerosol Composition and Sources with a Focus on Organic Nitrates. *Atmos. Chem. Phys.* **2015**, *15* (13), 7307–7336. https://doi.org/10.5194/acp-15-7307-2015.

(26) Xu, L.; Pye, H. O. T.; He, J.; Chen, Y.; Murphy, B. N.; Ng, N. L. Experimental and Model Estimates of the Contributions from Biogenic Monoterpenes and Sesquiterpenes to Secondary Organic Aerosol in the Southeastern United States. *Atmos. Chem. Phys.* **2018**, *18* (17), 12613–12637. https://doi.org/10.5194/acp-18-12613-2018.

(27) Lee, B. H.; Mohr, C.; Lopez-Hilfiker, F. D.; Lutz, A.; Hallquist, M.; Lee, L.; Romer, P.; Cohen, R. C.; Iyer, S.; Kurtén, T. et al. Highly Functionalized Organic Nitrates in the Southeast United States: Contribution to Secondary Organic Aerosol and Reactive Nitrogen Budgets. *Proc. Natl. Acad. Sci.* **2016**, *113* (6), 1516–1521. https://doi.org/10.1073/PNAS.1508108113.

(28) Zhang, H.; Yee, L. D.; Lee, B. H.; Curtis, M. P.; Worton, D. R.; Isaacman-VanWertz, G.; Offenberg, J. H.; Lewandowski, M.; Kleindienst, T. E.; Beaver, M. R. et al. Monoterpenes Are the Largest Source of Summertime Organic Aerosol in the Southeastern United States. *Proc. Natl. Acad. Sci. U. S. A.* **2018**, *115* (9), 2038–2043. https://doi.org/10.1073/pnas.1717513115.

(29) Schwantes, R.; Emmons, L.; Orlando, J.; Barth, M. C.; Tyndall, G. S.; Hall, S. R.; Ullmann, K.; St. Clair, J. M.; Blake, D. R.; Wisthaler, A. et al. Comprehensive Isoprene and Terpene Chemistry Improves Simulated Surface Ozone in the Southeastern U.S. *Atmos. Chem. Phys.* **2020**, *20*, 3739–3776. https://doi.org/10.5194/acp-2019-902.

(30) Browne, E. C.; Wooldridge, P. J.; Min, K. E.; Cohen, R. C. On the Role of Monoterpene Chemistry in the Remote Continental Boundary Layer. *Atmos. Chem. Phys.* **2014**, *14* (3), 1225–1238. https://doi.org/10.5194/acp-14-1225-2014.

(31) Wang, Y.; Piletic, I. R.; Takeuchi, M.; Xu, T.; France, S.; Ng, N. L. Synthesis and Hydrolysis of Atmospherically Relevant Monoterpene-Derived Organic Nitrates. *Environ. Sci. Technol.* **2021**, *55* (21), 14595–14606. https://doi.org/10.1021/acs.est.1c05310.

(32) Nichols, P. L.; Magnusson, A. B.; Ingham, J. D. Synthesis of Nitric Esters by the Addition of Nitric Acid to the Ethylene Oxide Ring. *J. Am. Chem. Soc.* **1953**, *75* (17), 4255–4258. https://doi.org/10.1021/ja01113a031.

(33) Muthuramu, K.; Shepson, P. B.; O'Brien, J. M. Preparation, Analysis, and Atmospheric Production of Multifunctional Organic Nitrates. *Environ. Sci. Technol.* **1993**, *27* (6), 1117–1124. https://doi.org/10.1021/es00043a010.

(34) Rollins, A. W.; Fry, J. L.; Hunter, J. F.; Kroll, J. H.; Worsnop, D. R.; Singaram, S. W.; Cohen, R. C. Elemental Analysis of Aerosol Organic Nitrates with Electron Ionization High-Resolution Mass Spectrometry. *Atmos. Meas. Tech.* **2010**, *3* (1), 301–310. https://doi.org/10.5194/amt-3-301-2010.

(35) Dess, D. B.; Martin, J. C. Readily Accessible 12-I-51 Oxidant for the Conversion of Primary and Secondary Alcohols to Aldehydes and Ketones. *J. Org. Chem.* **1983**, *48* (22), 4155–4156. https://doi.org/10.1021/jo00170a070.

(36) Filler, R. Oxidations and Dehydrogenations with N-Bromosuccinimide and Related n-Haloimides. *Chem. Rev.* **1963**, *63* (1), 21–43. https://doi.org/10.1021/cr60221a002.

(37) Kannan, N.; Rangaswamy, M. J.; Kemapaiah, B. B. Microwave Assisted Bi-Functional Activation of β-Bromo-Tert-Alcohols. *J. Chem. Sci.* **2015**, *127* (8), 1405–1410. https://doi.org/10.1007/s12039-015-0906-y.

(38) Treves, K.; Shragina, L.; Rudich, Y. Henry's Law Constants of Some β-, γ-, and δ-Hydroxy Alkyl Nitrates of Atmospheric Interest. *Environ. Sci. Technol.* **2000**, *34* (7), 1197–1203. https://doi.org/10.1021/es990558a.
(39) Nortcliffe, A.; Ekstrom, A. G.; Black, J. R.; Ross, J. A.; Habib, F. K.; Botting, N. P.; O'Hagan, D. Synthesis and Biological Evaluation of Nitric Oxide-Donating Analogues of Sulindac for Prostate Cancer Treatment. *Bioorganic Med. Chem.* **2014**, *22* (2), 756–761. https://doi.org/10.1016/j.bmc.2013.12.014.
(40) Yang, X.; Luo, F.; Li, J.; Chen, D.; Ye, E.; Lin, W.; Jin, J. Alkyl and Aromatic Nitrates in Atmospheric Particles Determined by Gas Chromatography Tandem Mass Spectrometry. *J. Am. Soc. Mass Spectrom.* **2019**, *30* (12), 2762–2770. https://doi.org/10.1007/s13361-019-02347-8.
(41) Boyd, C. M.; Sanchez, J.; Xu, L.; Eugene, A. J.; Nah, T.; Tuet, W. Y.; Guzman, M. I.; Ng, N. L. Secondary Organic Aerosol Formation from the β-Pinene+NO3 System: Effect of Humidity and Peroxy Radical Fate. *Atmos. Chem. Phys.* **2015**, *15* (13), 7497–7522. https://doi.org/10.5194/acp-15-7497-2015.
(42) Huang, Y.; Zhao, R.; Charan, S. M.; Kenseth, C. M.; Zhang, X.; Seinfeld, J. H. Unified Theory of Vapor-Wall Mass Transport in Teflon-Walled Environmental Chambers. *Environ. Sci. Technol.* **2018**, *52* (4), 2134–2142. https://doi.org/10.1021/acs.est.7b05575.
(43) Zhang, X.; Cappa, C. D.; Jathar, S. H.; McVay, R. C.; Ensberg, J. J.; Kleeman, M. J.; Seinfeld, J. H. Influence of Vapor Wall Loss in Laboratory Chambers on Yields of Secondary Organic Aerosol. *Proc. Natl. Acad. Sci. U. S. A.* **2014**, *111* (16), 5802–5807. https://doi.org/10.1073/pnas.1404727111.
(44) Krechmer, J. E.; Pagonis, D.; Ziemann, P. J.; Jimenez, J. L. Quantification of Gas-Wall Partitioning in Teflon Environmental Chambers Using Rapid Bursts of Low-Volatility Oxidized Species Generated in Situ. *Environ. Sci. Technol.* **2016**, *50* (11), 5757–5765. https://doi.org/10.1021/acs.est.6b00606.
(45) Zhang, X.; Schwantes, R. H.; McVay, R. C.; Lignell, H.; Coggon, M. M.; Flagan, R. C.; Seinfeld, J. H. Vapor Wall Deposition in Teflon Chambers. *Atmos. Chem. Phys.* **2015**, *15* (8), 4197–4214. https://doi.org/10.5194/acp-15-4197-2015.
(46) Nah, T.; McVay, R. C.; Pierce, J. R.; Seinfeld, J. H.; Ng, N. L. Constraining Uncertainties in Particle-Wall Deposition Correction during SOA Formation in Chamber Experiments. *Atmos. Chem. Phys.* **2017**, *17* (3), 2297–2310. https://doi.org/10.5194/acp-17-2297-2017.
(47) Boyd, C. M.; Nah, T.; Xu, L.; Berkemeier, T.; Ng, N. L. Secondary Organic Aerosol (SOA) from Nitrate Radical Oxidation of Monoterpenes: Effects of Temperature, Dilution, and Humidity on Aerosol Formation, Mixing, and Evaporation. *Environ. Sci. Technol.* **2017**, *51* (14), 7831–7841. https://doi.org/10.1021/acs.est.7b01460.
(48) Takeuchi, M.; Ng, N. L. Chemical Composition and Hydrolysis of Organic Nitrate Aerosol Formed from Hydroxyl and Nitrate Radical Oxidation of α-Pinene and β-Pinene. *Atmos. Chem. Phys.* **2019**, *19* (19), 12749–12766. https://doi.org/10.5194/acp-19-12749-2019.
(49) Chen, Y.; Takeuchi, M.; Nah, T.; Xu, L.; Canagaratna, M. R.; Stark, H.; Baumann, K.; Canonaco, F.; Prevot, A. S. H.; Gregory Huey, L. et al. Chemical Characterization of Secondary Organic Aerosol at a Rural Site in the Southeastern US: Insights from Simultaneous High-Resolution Time-of-Flight Aerosol Mass Spectrometer (HR-ToF-AMS) and FIGAERO Chemical Ionization Mass Spectrometer (CIMS) Measur. *Atmos. Chem. Phys.* **2020**, *20* (14), 8421–8440. https://doi.org/10.5194/acp-20-8421-2020.
(50) Sadanaga, Y.; Takaji, R.; Ishiyama, A.; Nakajima, K.; Matsuki, A.; Bandow, H. Thermal Dissociation Cavity Attenuated Phase Shift Spectroscopy for Continuous Measurement of Total Peroxy and Organic Nitrates in the Clean Atmosphere. *Rev. Sci. Instrum.* **2016**, *87* (7). https://doi.org/10.1063/1.4958167.
(51) Lerosen, A. L.; Reid, C. E. An Investigation of Certain Solvent Effect in Absorption Spectra. *J. Chem. Phys.* **1952**, *20* (2), 233–236. https://doi.org/10.1063/1.1700384.
(52) Wang, S.; Pratt, K. A. Molecular Halogens Above the Arctic Snowpack: Emissions, Diurnal

Variations, and Recycling Mechanisms. *J. Geophys. Res. Atmos.* **2017**, *122* (21), 11,991-12,007. https://doi.org/10.1002/2017JD027175.
(53) Wang, S.; McNamara, S. M.; Moore, C. W.; Obrist, D.; Steffen, A.; Shepson, P. B.; Staebler, R. M.; Raso, A. R. W.; Pratt, K. A. Direct Detection of Atmospheric Atomic Bromine Leading to Mercury and Ozone Depletion. *Proc. Natl. Acad. Sci. U. S. A.* **2019**, *116* (29), 14479–14484. https://doi.org/10.1073/pnas.1900613116.
(54) Cohen, S. D.; Hindmarsh, A. C. *CVODE User Guide*; Lawrence Livermore National Laboratory report UCRLMA-118618, 1994.
(55) Vereecken, L.; Peeters, J. Decomposition of Substituted Alkoxy Radicals - Part I: A Generalized Structure-Activity Relationship for Reaction Barrier Heights. *Phys. Chem. Chem. Phys.* **2009**, *11* (40), 9062–9074. https://doi.org/10.1039/b909712k.
(56) Vereecken, L.; Peeters, J. A Structure-Activity Relationship for the Rate Coefficient of H-Migration in Substituted Alkoxy Radicals. *Phys. Chem. Chem. Phys.* **2010**, *12* (39), 12608–12620. https://doi.org/10.1039/c0cp00387e.
(57) Skoog, D. A.; West, D. M.; Holler, F. J.; Crouch, S. R. *Fundamentals of Analytical Chemistry, 9th Edition*; Boston, 2014.
(58) Jenkin, M. E.; Saunders, S. M.; Wagner, V.; Pilling, M. J. Protocol for the Development of the Master Chemical Mechanism, MCM v3 (Part B): Tropospheric Degradation of Aromatic Volatile Organic Compounds. *Atmos. Chem. Phys.* **2003**, *3* (1), 181–193. https://doi.org/10.5194/acp-3-181-2003.
(59) Jenkin, M. E.; Saunders, S. M.; Pilling, M. J. The Tropospheric Degradation of Volatile Organic Compounds: A Protocol for Mechanism Development. *Atmos. Environ.* **1997**, *31* (1), 81–104. https://doi.org/10.1016/S1352-2310(96)00105-7.
(60) Tadić, J.; Juranić, I.; Moortgat, G. K. Pressure Dependence of the Photooxidation of Selected Carbonyl Compounds in Air: N-Butanal and n-Pentanal. *J. Photochem. Photobiol. A Chem.* **2001**, *143* (2–3), 169–179. https://doi.org/10.1016/S1010-6030(01)00524-X.
(61) Gardner, E. P.; Sperry, P. D.; Calvert, J. G. Primary Quantum Yields of NO2 Photodissociation. *J. Geophys. Res.* **1987**, *92* (2), 6642–6652.
(62) Roberts, J. M.; Fajer, R. W. UV Absorption Cross Sections of Organic Nitrates of Potential Atmospheric Importance and Estimation of Atmospheric Lifetimes. *Environ. Sci. Technol.* **1989**, *23* (8), 945–951.
(63) Romonosky, D. E.; Nguyen, L. Q.; Shemesh, D.; Nguyen, T. B.; Epstein, S. A.; Martin, D. B. C.; Vanderwal, C. D.; Gerber, R. B.; Nizkorodov, S. A. Absorption Spectra and Aqueous Photochemistry of β-Hydroxyalkyl Nitrates of Atmospheric Interest. *Mol. Phys.* **2015**, *113* (15–16), 2179–2190. https://doi.org/10.1080/00268976.2015.1017020.
(64) Talukdar, R. K.; Burkholder, J. B.; Hunter, M.; Gilles, M. K.; Roberts, J. M.; Ravishankara, A. R. Atmospheric Fate of Several Alkyl Nitrates. *J. Chem. Soc., Faraday Trans.* **1997**, *93* (16), 2797–2805.
(65) Xu, L.; Møller, K. H.; Crounse, J. D.; Otkjær, R. V.; Kjaergaard, H. G.; Wennberg, P. O. Unimolecular Reactions of Peroxy Radicals Formed in the Oxidation of α-Pinene and β-Pinene by Hydroxyl Radicals. *J. Phys. Chem. A* **2019**, *123* (8), 1661–1674. https://doi.org/10.1021/acs.jpca.8b11726.
(66) Vereecken, L.; Peeters, J. Nontraditional (per)Oxy Ring-Closure Paths in the Atmospheric Oxidation of Isoprene and Monoterpenes. *J. Phys. Chem. A* **2004**, *108* (24), 5197–5204. https://doi.org/10.1021/jp049219g.
(67) Vereecken, L.; Müller, J. F.; Peeters, J. Low-Volatility Poly-Oxygenates in the OH-Initiated Atmospheric Oxidation of α-Pinene: Impact of Non-Traditional Peroxyl Radical Chemistry. *Phys. Chem. Chem. Phys.* **2007**, *9* (38), 5241–5248. https://doi.org/10.1039/b708023a.
(68) Claflin, M. S.; Ziemann, P. J. Identification and Quantitation of Aerosol Products of the Reaction of β-Pinene with NO3 Radicals and Implications for Gas- and Particle-Phase Reaction Mechanisms. *J. Phys. Chem. A* **2018**, *122* (14), 3640–3652.

https://doi.org/10.1021/acs.jpca.8b00692.
(69) Huey, L. G. MEASUREMENT OF TRACE ATMOSPHERIC SPECIES BY CHEMICAL IONIZATION MASS SPECTROMETRY: SPECIATION OF REACTIVE NITROGEN AND FUTURE DIRECTIONS. *Mass Spectrom. Rev.* **2007**, No. 26, 166–184. https://doi.org/10.1002/mas.
(70) McNeill, V. F.; Wolfe, G. M.; Thornton, J. A. The Oxidation of Oleate in Submicron Aqueous Salt Aerosols: Evidence of a Surface Process. *J. Phys. Chem. A* **2007**, *111* (6), 1073–1083. https://doi.org/10.1021/jp066233f.
(71) Zhao, R.; Lee, A. K. Y.; Abbatt, J. P. D. Investigation of Aqueous-Phase Photooxidation of Glyoxal and Methylglyoxal by Aerosol Chemical Ionization Mass Spectrometry: Observation of Hydroxyhydroperoxide Formation. *J. Phys. Chem. A* **2012**, *116* (24), 6253–6263. https://doi.org/10.1021/jp211528d.
(72) Kebabian, P. L.; Wood, E. C.; Herndon, S. C.; Freedman, A. An Alternative Approach to Monitoring Nitrogen Dioxide: Cavity Attenuated Phase Shift Spectroscopy. *Air Waste Manag. Assoc. Symp. Air Qual. Meas. Methods Technol. 2008* **2008**, *42* (16), 214–218.
(73) Claflin, M. S.; Ziemann, P. J. Identification and Quantitation of Aerosol Products of the Reaction of β-Pinene with NO3 Radicals and Implications for Gas- and Particle-Phase Reaction Mechanisms. *J. Phys. Chem. A* **2018**, *122* (14), 3640–3652. https://doi.org/10.1021/acs.jpca.8b00692.
(74) Meyrahn, H.; Moortgat, G. K.; Warneck, P. The Photolysis of Acetaldehyde Under Atmospheric Conditions BT - Atmospheric Trace Constituents: Proceedings of the 5th Two-Annual Colloquium of the Sonderforschungsbereich 73 of the Universities Frankfurt and Mainz and the Max-Planck-Institut Mainz, Hel; Herbert, F., Ed.; Vieweg+Teubner Verlag: Wiesbaden, 1982; pp 65–72. https://doi.org/10.1007/978-3-322-90097-5_6.
(75) Wennberg, P. O.; Bates, K. H.; Crounse, J. D.; Dodson, L. G.; McVay, R. C.; Mertens, L. A.; Nguyen, T. B.; Praske, E.; Schwantes, R. H.; Smarte, M. D. et al. Gas-Phase Reactions of Isoprene and Its Major Oxidation Products. *Chem. Rev.* **2018**, *118* (7), 3337–3390. https://doi.org/10.1021/acs.chemrev.7b00439.
(76) Chen, J.; Møller, K. H.; Wennberg, P. O.; Kjaergaard, H. G. Unimolecular Reactions Following Indoor and Outdoor Limonene Ozonolysis. *J. Phys. Chem. A* **2021**, *125* (2), 669–680. https://doi.org/10.1021/acs.jpca.0c09882.
(77) Møller, K. H.; Otkjær, R. V.; Chen, J.; Kjaergaard, H. G. Double Bonds Are Key to Fast Unimolecular Reactivity in First-Generation Monoterpene Hydroxy Peroxy Radicals. *J. Phys. Chem. A* **2020**, *124* (14), 2885–2896. https://doi.org/10.1021/acs.jpca.0c01079.
(78) Card, M. L.; Gomez-Alvarez, V.; Lee, W. H.; Lynch, D. G.; Orentas, N. S.; Lee, M. T.; Wong, E. M.; Boethling, R. S. History of EPI Suite™ and Future Perspectives on Chemical Property Estimation in US Toxic Substances Control Act New Chemical Risk Assessments. *Environ. Sci. Process. Impacts* **2017**, *19* (3), 203–212. https://doi.org/10.1039/c7em00064b.
(79) Huang, W.; Saathoff, H.; Shen, X.; Ramisetty, R.; Leisner, T.; Mohr, C. Chemical Characterization of Highly Functionalized Organonitrates Contributing to Night-Time Organic Aerosol Mass Loadings and Particle Growth. *Environ. Sci. Technol.* **2019**, *53* (3), 1165–1174. https://doi.org/10.1021/acs.est.8b05826.

Table 1. Summary of photolysis rate constants.

ONs	Structures	$J_{chamber}$ ($\times 10^{-5}$ s^{-1})[a]	$\tau_{chamber}$ (h)[b]	Average quantum yield[c]	$J_{ambient}$ ($\times 10^{-5}$ s^{-1})[c,d,e]	$\tau_{ambient}$ (h)[c,d,e]	Cutoff wavelength (nm)[c,f]	$J_{ambient}$ ($\times 10^{-5}$ s^{-1})[c,d,h]	$\tau_{ambient}$ (h)[c,d,h]
Nitrooxyacetone	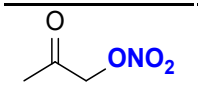	0.29 ± 0.11	95 ± 36	0.50 ± 0.21	1.7 ± 0.73	16 ± 6.9	/	/	/
3°_ApHN	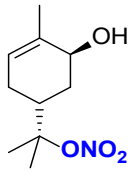	2.3 ± 0.80	12 ± 4.2	0.23 ± 0.11	8.3 ± 4.0	3.3 ± 1.6	330 ± 5	14 ± 6.7	2.0 ± 0.96
2°_LmHN	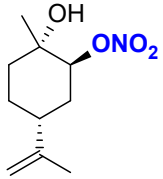	1.3 ± 0.50	21 ± 8.1	0.071 ± 0.035	3.0 ± 1.5	9.2 ± 4.5	325 ± 4	8.1 ± 4.0	3.4 ± 1.7
1°_BpHN	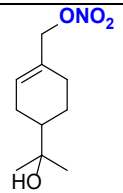	0.55 ± 0.10	51 ± 9.3	0.038 ± 0.013	1.7 ± 0.60	17 ± 6.0	312 ± 1	4.1 ± 1.4	6.8 ± 2.4

[a.] The uncertainties were propagated from the statistical errors associated with k_{vwl} and k_{O3}; [b.] The uncertainties were propagated from the uncertainties of $J_{chamber}$; [c.] The uncertainties were propagated from $j_{chamber}$, instrumental uncertainty (5%) of measured spectral photon flux, and the average of measured absorption cross sections from different solution concentrations; [d.] Solar spectral photon flux was from TUV-radiation model, solar zenith angle of 28.14°, 12:00 solar time, August 1 at 33.75° latitude north (Atlanta), overhead O_3 column 300 Du, and albedo 0.1; [e.] The ambient photolysis rate constants and lifetimes were calculated based on average quantum yields; [f.] For wavelength ≤ cutoff wavelength, quantum yield = 1; Otherwise, quantum yield = 0; [h.] The ambient photolysis rate constants and lifetimes were calculated based on wavelength-dependent quantum yields.

Table 2. Comparison of photolysis, photooxidation, and ozonolysis lifetimes of MT-ONs.

ONs	3°_ApHN		2°_LmHN		1°_BpHN	
Structures	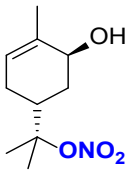		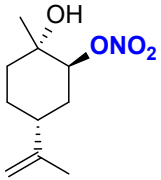		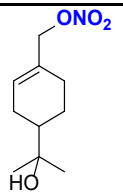	
Rate constant for reaction with OH (10^{-11} cm^3 $molec^{-1}$ s^{-1})	9.9[a]		5.9[a]		5.7[b]	
Photooxidation lifetime ([OH] = 1.5×10^6 molec cm^{-3})	1.9 h		3.1 h		3.2 h	
Rate constant for reaction with O_3 (10^{-16} cm^3 $molec^{-1}$ s^{-1})	4.2[c]		1.7[c]		1.1[c]	
Ozonolysis lifetime ([O_3] = 50 ppb)	5.3 h		13 h		20 h	
Photolysis rate constant (10^{-5} s^{-1})	8.3[d]	14[e]	3.0[d]	8.1[e]	1.7[d]	4.1[e]
Photolysis lifetime	3.3[d] h	2.0[e] h	9.2[d] h	3.4[e] h	17[d] h	6.8[e] h

[a.] Master Chemical Mechanism (version 3.3.1); [b.] Estimation Program Interface suite (EPI Suite™, https://www.epa.gov/tsca-screening-tools/epi-suitetm-estimation-program-interface); [c.] Separate ozonolysis experiments of MT-ONs; [d.] The ambient photolysis rate constants and lifetimes were calculated based on average quantum yields; [e.] The ambient photolysis rate constants and lifetimes were calculated based on wavelength-dependent quantum yields.

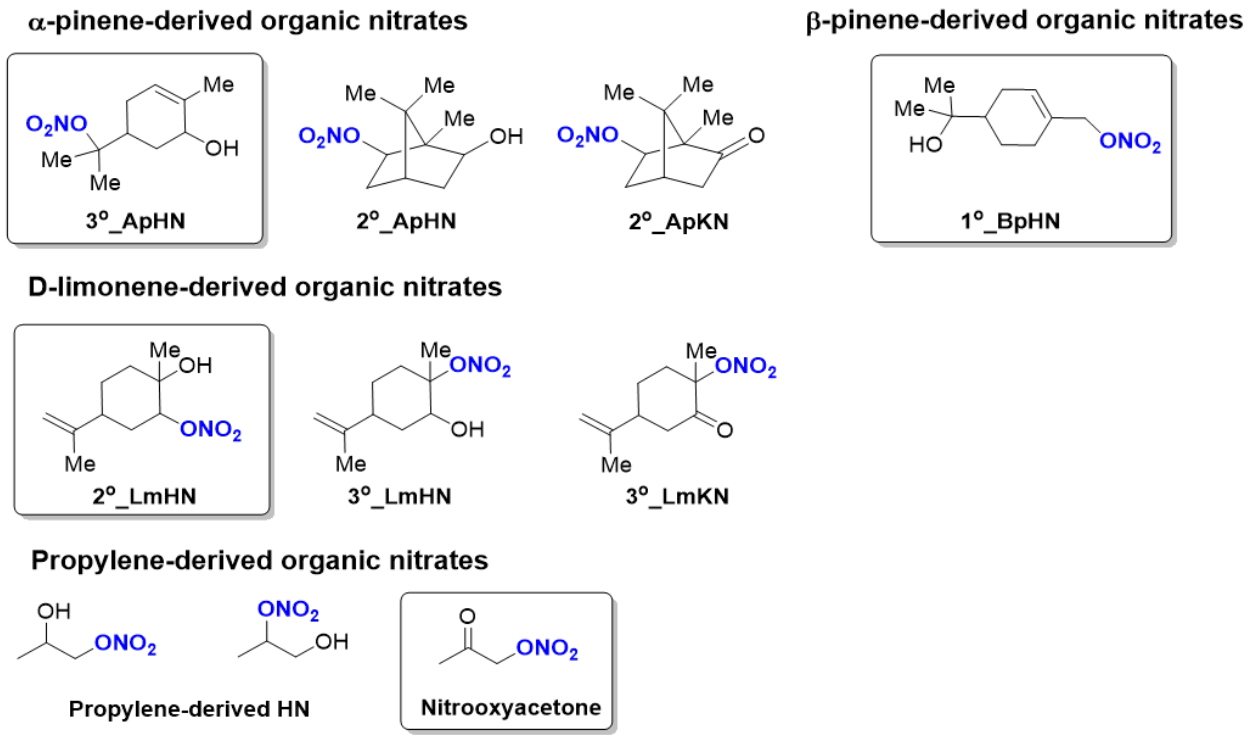

Figure 1. Molecular structures of ONs (HN: hydroxy nitrates and KN: keto-nitrates) synthesized in this work and their abbreviations. The numbers (1°, 2°, and 3°) in the abbreviations denote a primary, secondary, and tertiary nitrooxy group, respectively. The ONs in the boxes were introduced into the chamber to study the photolysis process.

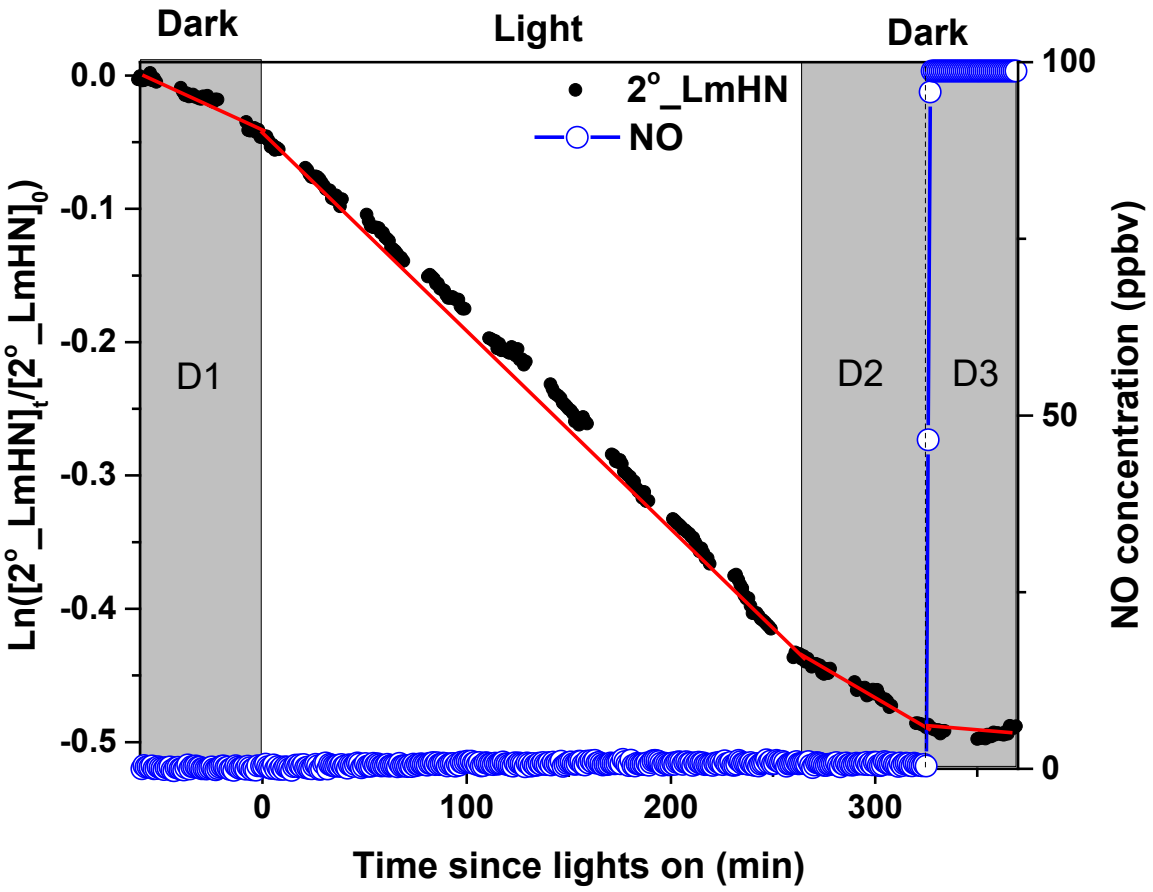

Figure 2. First-order kinetics analysis for photolysis of 2º_LmHN. The red line in each period corresponds to first-order kinetics-fitting curve. **D1** is the dark period before irradiation time (light on). **D2** and **D3** are dark periods after irradiation time. Detailed discussion for each period is provided in section 2.2.

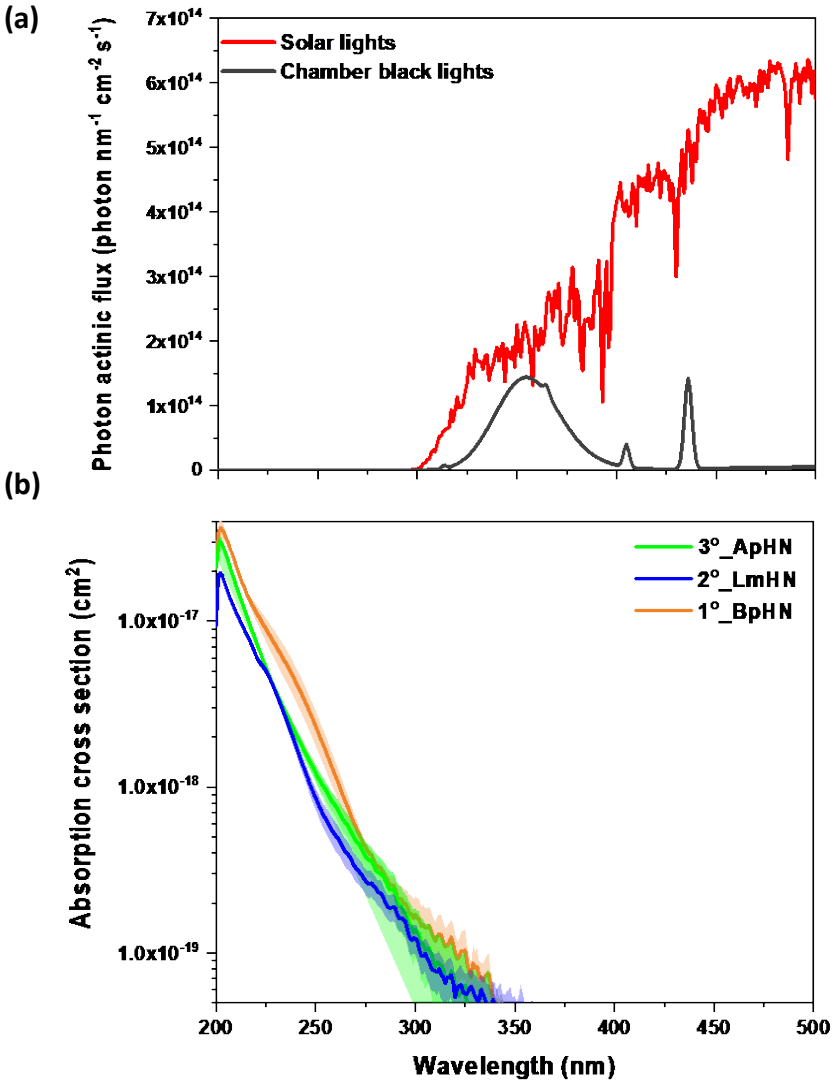

Figure 3. (a) Comparison between GTEC chamber black lights and solar spectral photon flux (extracted from TUV-radiation model, solar zenith angle of 28.14°, 12:00 solar time, August 1 at 33.75° latitude north (Atlanta), overhead O_3 column 300 Du, and albedo 0.1); (b) Absorption cross sections of 3°_ApHN, 2°_LmHN, and 1°_BpHN in ethyl ether. The uncertainties in the shaded areas were from the average of measured absorption cross sections in different solution concentrations.

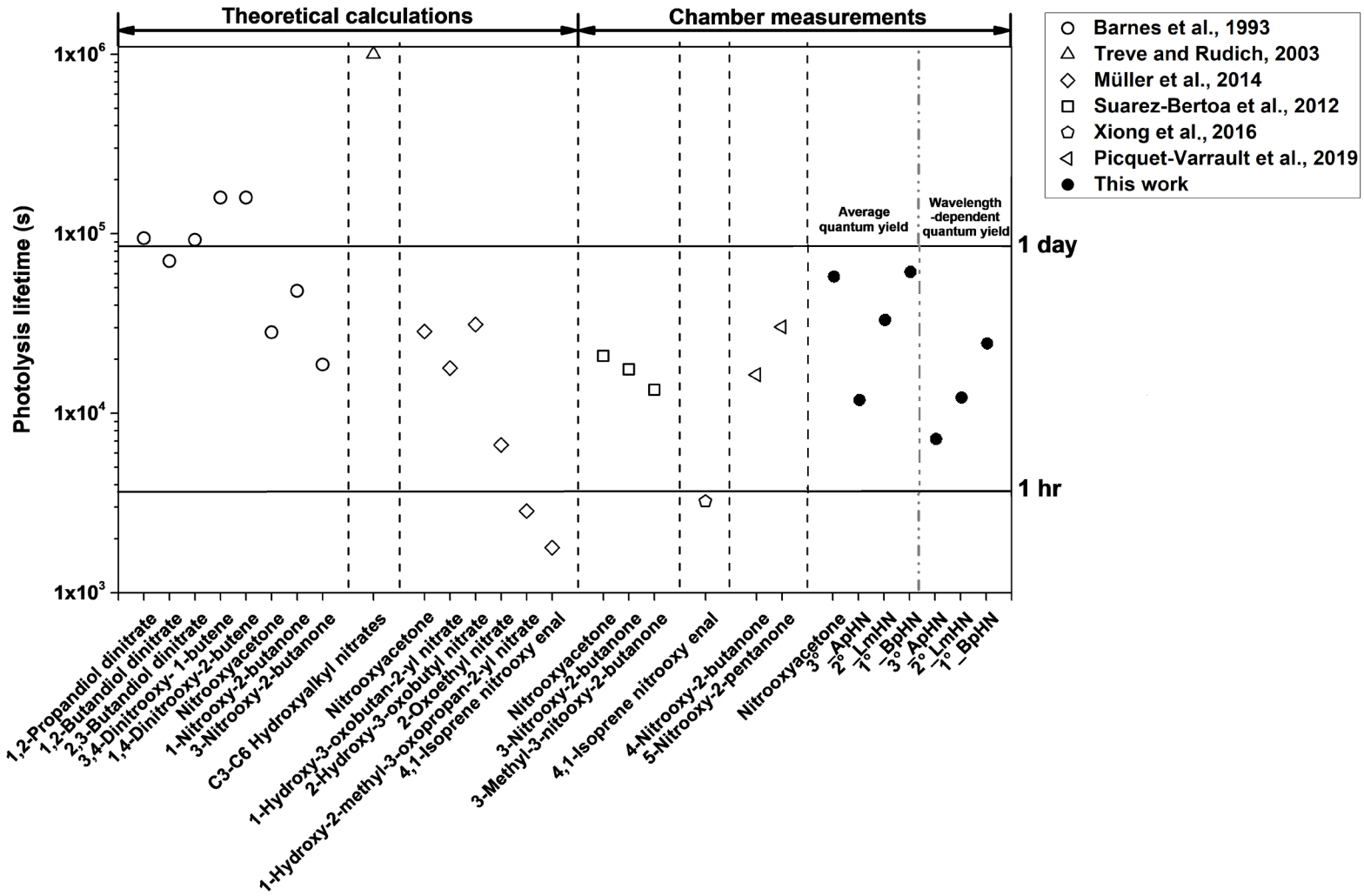

Figure 4. Photolysis lifetimes reported in this study and in the literature[8–12,15] (corresponding to Table S3).

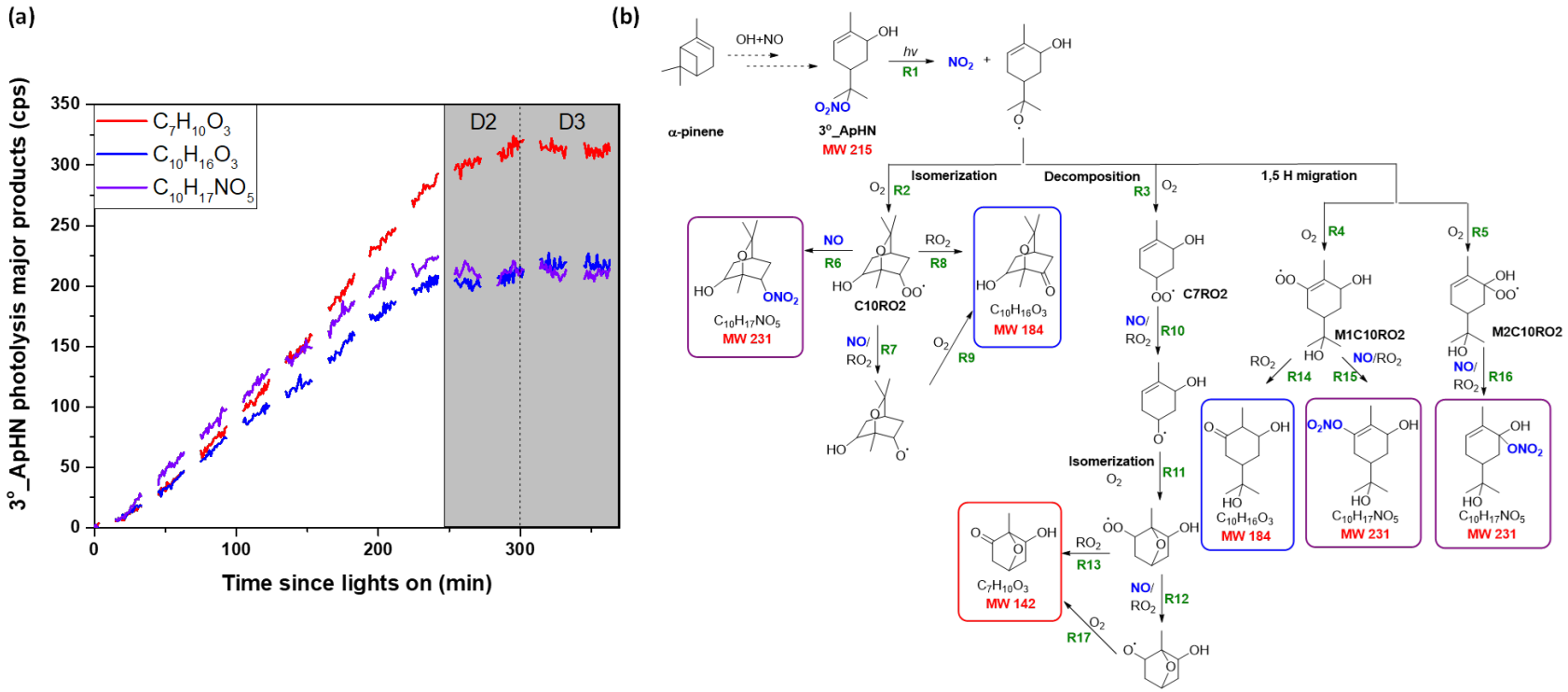

Figure 5. (a) Time series of the major gas-phase products from photolysis of 3°_ApHN measured by the HR-ToF-CIMS. **D2** and **D3** are dark periods after irradiation time. Detailed discussion for each period is provided in sections 2.2; (b) Proposed mechanisms for the formation of major gas-phase products from photolysis of 3°_ApHN. The compounds in the boxes are major gas-phase products identified by HR-ToF-CIMS.

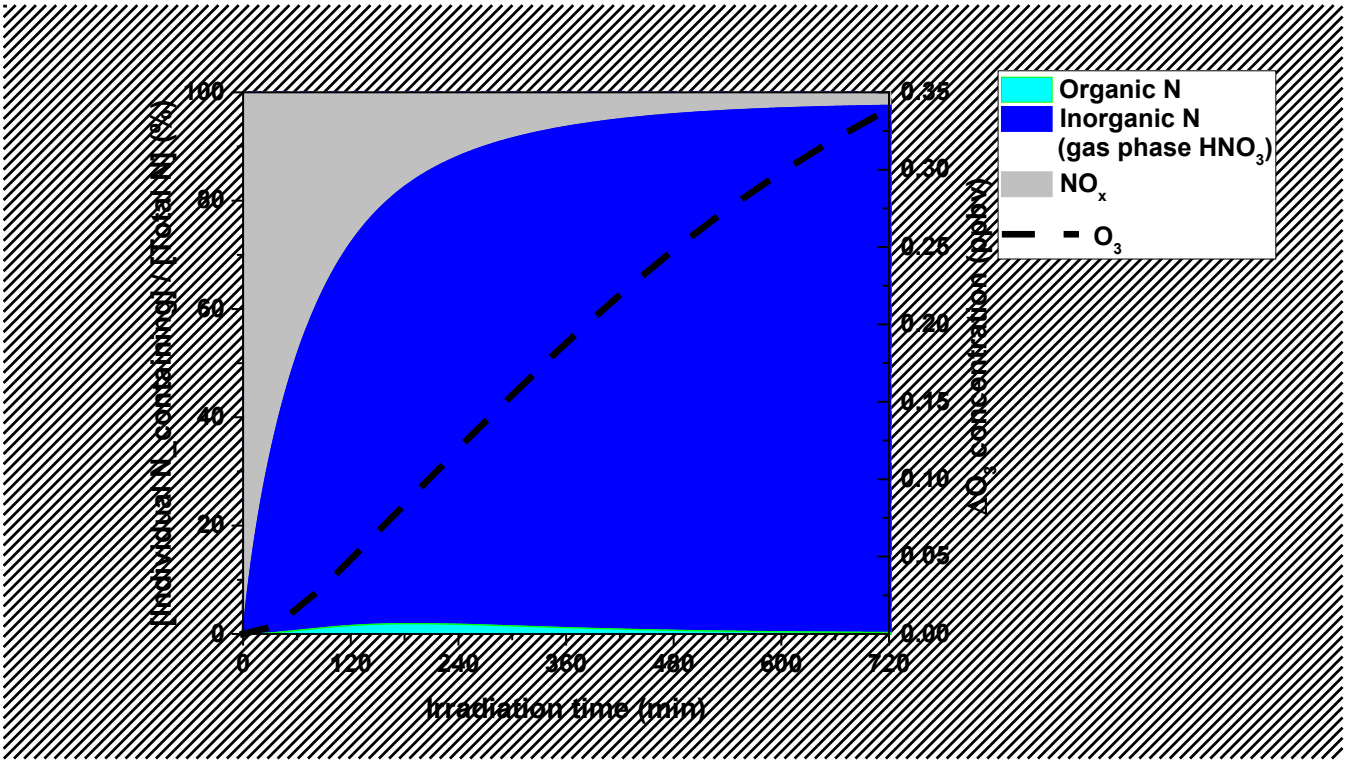

Figure 6. Nitrogen conversion during photolysis of 3º_ApHN (28 pptv) with an initial O_3 concentration of 46 ppbv.

TOC Graphic